Large two phase Digital Rock Physics simulations for relative permeability uncertainty assessment

Mohamed Regaieg[1*], *Igor* Bondino[2], *Clément* Varloteaux[3], *Titly* Farhana Faisal[4], *Jianhui* Yang[5] and *Richard* Rivenq[1]

[1] TotalEnergies SE, Pau, France

[2] TotalEnergies SE, Feluy, Belgium

[3] Computational Hydrocarbon Laboratory for Optimized Energy Efficiency, Pau, France

[4] National Institute for Research in Computer Science and Automation, Pau, Francessssss

[5] TotalEnergies E&P, Aberdeen, United Kingdom

Abstract

Recent numerical developments in digital rock physics, known as Generalized Network Modelling (GNM) [25], allow to reconstruct an upscaled version of the 3D segmented image of a rock in the form of a network of pore elements where the single-phase flow conductances in each pore are derived by solving the Stokes equation in the original geometry. In engineering terms, this hybrid solution allows to capture relevant flow information from the original Micro-CT image whilst keeping the overall cost of multi-phase computation manageable. In this work, OpenFOAM is called for the Stokes flow solution inside a pore network extraction platform called GNextract developed with Imperial College, London, during a 8-year collaboration [25], and TOTAL's pore-scale network simulator DynaPNM [27] is used in quasi-static mode after having been made fully parallel. All codes are run on TOTAL's supercomputer PANGEA.

In the first part of this paper we give an overview of TOTAL's two-phase flow simulation workflow. We then continue on the physics side reporting a new major finding with respect to assumptions that have been used so far by the majority of authors for the modelling of water layers in mixed-to-oil wet rocks. This is seen to have a very large impact on simulation accuracy, especially in terms of relative permeability trends versus wettability. Subsequently, we validate our simulation workflow against three relative permeability experiments performed on microplugs and against a SCAL dataset. The comparison against all datasets gave satisfactory results. On the computational side, we describe how we are able to extract and simulate large networks thanks to a newly developed stitching algorithm and to the parallelization of our pore scale simulator. This allowed us to perform large uncertainty studies (thousands simulations / day) on images as large as (8480x8480x10000) voxels representing a rock volume of 46 cm^3. Being able to simulate large networks allowed us to study the impact of the image size on the spread of the simulated residual oil saturation. We show that simulations on images as small as 1200x1200x1200 are dominated by finite size effect and result on large variability of the simulations. This finite size effect is drastically reduced by simulating much larger images, greatly improving the precision of the numerical result.

1- Introduction

Digital Rock Physics (DRP) has been an appealing technology to the oil and gas industry in the last 25 years. In fact, oil and gas companies have dreamt of using DRP as a mean to predict multi-phase properties of Reservoir Rocks (such as Kr and Pc) numerically without the need to perform SCAL experiments. However, the problem has proved more complex than what researchers have expected, and the weakest points of the technology have been the limitation of image resolution [29], rock/fluids wettability characterization [7, 32] and sometimes an over-simplification of the physics. DRP could also be criticized for computing properties on usually small rock volumes without proving neither that the Representative Elementary Volume (REV) for single phase and two-phase flow is reached nor that the simulations are not dominated by finite size and boundary effects.

Advances in Micro-CT imaging have allowed the characterization of wettability from images of multiphase flow experiments. Andrew et al [4] have measured the contact angles manually in scCO2-Brine-Carbonate system by tracing vectors tangential to the solid surface and the scCO2–brine interface. This was done at 300 locations on an image of scCO2 trapped as a residual phase in the pore-space of the scCO2. In more recent works, other researchers have developed automatic contact angle computation methods [3, 30]. These methods were used to compute contact angles either at residual oil saturation Sor [2] or after stabilization of co-injection of water and oil [13].

Several simulation techniques have been developed to study single and two-phase flow in porous media. Direct numerical simulation (DNS) methods such as finite volume method and Lattice Boltzmann have been widely used to compute petrophysical properties of rocks directly on Micro-CT images [24, 35]. However, these methods

* Corresponding author: regaieg.mohamed@gmail.com

are computationally expensive for two-phase and capillary dominated flow regime which characterizes most oil reservoirs. Pore Network modelling (PNM) technique, on the other hand, simplifies the pore structure and idealizes its geometry through a pore network extraction [10] that is later used in a pore network simulator to compute single and two-phase flow properties [26]. The latter technique is very efficient computationally and can be used to simulate larger volumes [27]. However, the older models [22, 34] used empirical models and geometry simplifications to compute the node to node conductivities which is a critical parameter in petrophysical properties computations. In this work, we take the best of both approaches. First, a single-phase DNS simulation is performed on the rock image and coupled with a pore network extraction. This results in a pore network with conductivities measured on the original geometry [25]. Subsequently, PNM simulations are used to perform two-phase flow simulations using TOTAL's quasi-static pore-scale network simulator DynaPNM [27]. The film flow physics in oil and mixed-wet scenarios have been revisited compared to the models used by most of the authors [28, 34] that can have a major impact on relative permeability. Furthermore, DynaPNM has been parallelized allowing us to simulate large volumes and thus to avoid finite size effects and to get as close as possible to the REV for single and two-phase flow.

In this paper, we describe TOTAL's DRP workflow based on 1) GNM technique to extract a pore network with conductivities computed on the rock image, 2) a network stitching code that allows the extraction of larger networks and 3) TOTAL's fully parallelized inhouse tool DynaPNM that can simulate several million networks with several million pore elements extracted from images as large as 8480*8480*10000 voxels. During the simulation exercise, we perform sensitivity studies that vary the uncertain parameters of the simulations. Thousands of different realizations are used to produce P10, P50 and P90 relative permeability sets. This workflow is then applied to several outcrop and reservoir rocks and allows us to conclude of the state of the art of this technology.

2 Description of the simulation workflow

2.1 Pore network extraction

In contrast to some digital rock physics methods, pore network models do not involve two-phase direct flow simulation in a 3D CT image or a reconstructed digital rock. Instead, it needs a pore network that is extracted from 3D reconstructions. Various algorithms exist to extract the skeleton of the 3D model that carries the essential geometric and topological information of the underlying pore system. In this work, we use a pore network extraction platform called GNextract developed with Imperial College, London, during an 8-year collaboration [25]. GNextract is first used to reconstruct an upscaled version of the 3D segmented image of a rock in the form of a network of pore elements where the single-phase flow conductances in each pore are derived by solving the Stokes equation in the original geometry using OpenFOAM. Unfortunately, the extraction code needs large amount of memory to extract large images (more than 60 GB of RAM for 1500^3 voxels image). Furthermore, although OpenFOAM simulations are parallelized, they are computationally expensive and require a large amount of resources and/or simulation time for large images. Therefore, to overcome these limitations, a stitching process has been developed on networks extracted from overlapped sub-volume of a given image (Figure 1). Figure 1 illustrates the stitching process and shows that the stitched network is formed by a first part conserved from PNM1, a second part conserved from PNM2 and a third part obtained on a transition zone where rules inspired from the ones used by GNextract are defined to choose the elements to conserve --some elements being obtained from PNM1 whilst others from PNM2. In the transition zone, if several pore elements are obtained to describe the same feature, only the largest pore bodies and largest pore throats are kept. This is motivated by the fact that the extraction algorithm computes each element size from the largest inscribed sphere in the porous space. Therefore, the extraction algorithm tends to naturally choose the widest space available for determining element size. If a large extraction is required, several stitching operations are performed thus reducing the memory usage and accelerating the computations.

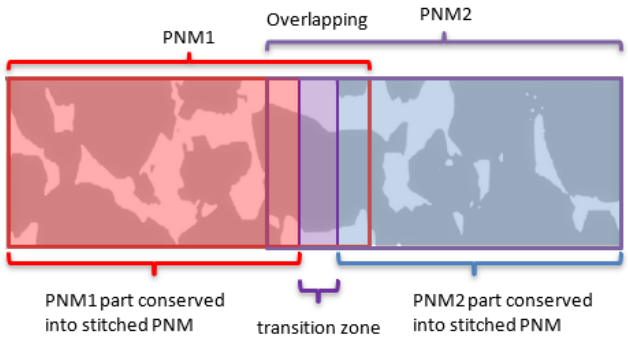

Figure 1 : An illustration of the pore network stitching process

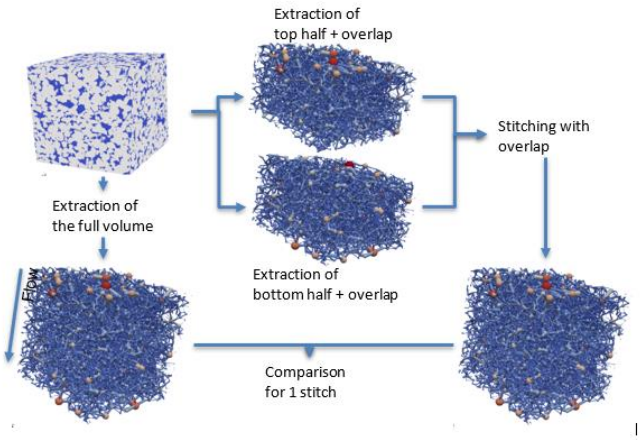

Figure 2: Illustration of the validation of the stitching code

In order to validate the stitching algorithm, we have compared waterflood relative permeability curves from a

reference case in which we extract a pore network from the full image to a stitched pore network from the same image with varying transition length (Figure 2). For the tested rocks (Figure 2), the absolute permeability varied by less than 5% and the waterflood relative permeability in the stitched networks agreed well with the reference network (Figures 4 and 5). In the simulations of Figures 4 and 5, an image 2000x1000x1000 have been used corresponding to network sizes of 10000 nodes and 100000 nodes respectively for rock A and B, An overlap, from 200 to 1600 voxels have been used and constant contact angles were considered (140° for OW and 50° for WW).

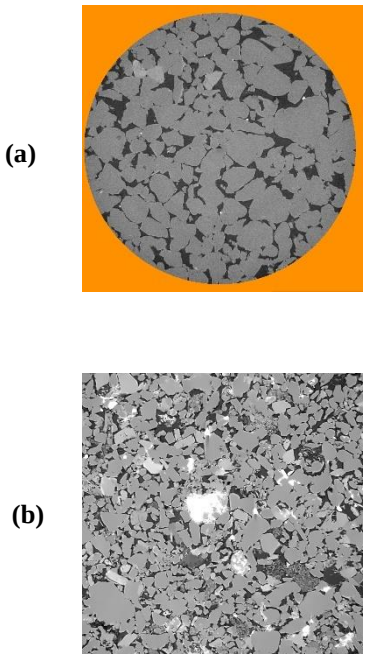

Figure 3 : Micro-CT images of Sandstone Reservoir Rocks used in this paper, clean sandstone that we call Reservoir Sandstone A (a) and Sandstone with clay that we call Reservoir Sandstone B (b)

2.2 Pore network flow simulator

2.2.1 DynaPNM: a parallel pore network simulator

Once a pore network is extracted with the corresponding conductance values from single phase DNS simulation, we go on to perform two-phase flow simulations. These simulations are performed using DynaPNM, TOTAL's inhouse pore network simulator [27], that we use in quasi-static mode as all the cases that we study in this paper are capillary dominated.

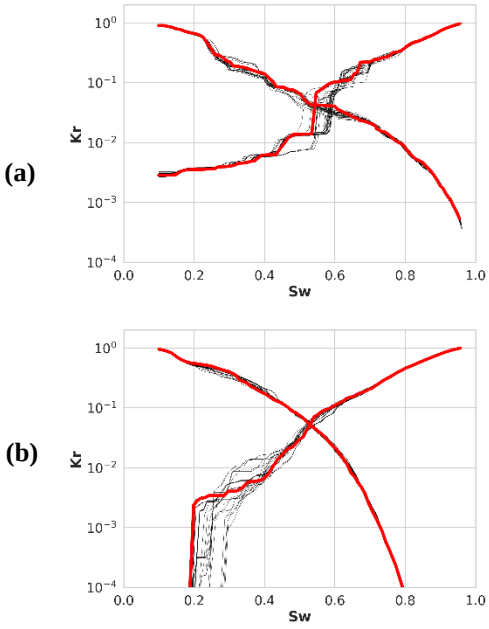

Figure 4 : Comparison of waterflood relative permeability curves of the stitched (black) and reference (red) pore networks for an oil-wet scenario for Reservoir Sandstone A (a) and Reservoir Sandstone B (b)

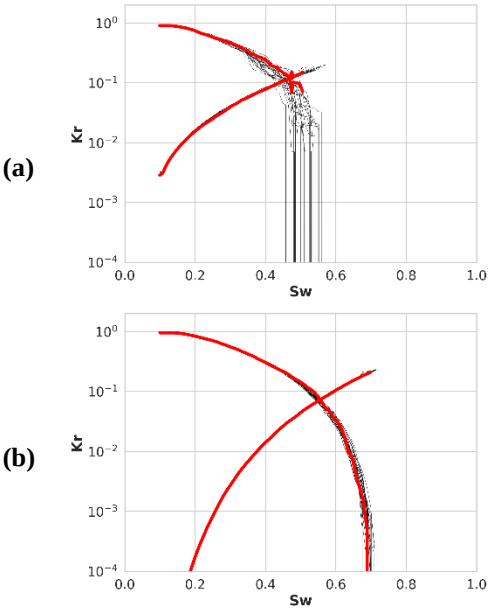

Figure 5 : Comparison of waterflood relative permeability curves of the stitched (black) and reference (red) pore networks for a water-wet scenario for Reservoir Sandstone A (a) and Reservoir Sandstone B (b)

The physical rules implemented in the simulator are broadly similar to the ones used in [22, 34] with the exception of a major change in the film flow model which is presented in the next section. The geometry of the pore network is simplified into an ensemble of pore bodies connected through pore throats during the pore network extraction step. As the invasions are totally controlled by the geometry, there is no need to compute the pressure gradients. The invasion order is determined through the

capillary entry pressure of each element and the trapping is determined through a clustering algorithm. For every relative permeability point computation, the phases are isolated, and a pressure drop is applied to the network. The pressure is then solved, the corresponding production rate is computed, and effective permeability of each phase is determined through Darcy's law.

The network is initially filled with water. A primary drainage is first simulated in order to establish irreducible water saturation, Swi. As the network is assumed water-wet, oil injection follows an invasion percolation regime. Water layers in pore elements with corners make water trapping very difficult and allow to achieve very low Swi values.

Primary drainage is then followed with a waterflood after an aging process where oil filled pore wettability is changed — water filled pores remain water-wet. We note here that we enter receding contact angle distributions in primary drainage and advancing contact angle distributions in waterflood. First, water spontaneously fills the water-wet part of the network through piston like displacement and snap-off. In this phase the smallest pores are filled first, then the next smallest are filled, and so on. The defending oil phase can escape by flowing through oil-filled pores. Once spontaneous imbibition ends, the invading water is over pressured by applying a negative capillary pressure. Now, the largest pore elements are filled first, and oil can escape to the outlet either by flowing through the center of oil filled pores or through oil films. Once all the oil is trapped, the simulation stops.

The simulator has been parallelized to allow the simulation of large systems. First, the domain is decomposed, each processor is allocated memory and performs the computations of a subdomain. Each processor needs also information from the neighboring subdomains and this information is stored by each processor. The pore bodies and throats inside each subdomain of a processor are named local elements while the pore bodies and throats from neighbor subdomains are named ghost elements. Synchronization of the information of the ghost elements is performed after each capillary pressure step or after a maximum change in the network phases saturations. This communication is made using Message Passing Interface library MPI [14]. Furthermore, a parallel clustering algorithm has been implemented in order to determine if the defending phase is trapped and parallel linear solver library [6] is used for permeability and relative permeability computations.

We propose to test the accuracy and the robustness of our parallel pore network simulator for several networks and wettability scenarios. We consider two pore networks, the first is extracted from a Reservoir sandstone that we call Reservoir Sandstone B (320000 pore elements) and from a very heterogenous carbonate network that we call Reservoir Carbonate C (1 million pore elements). Subsequently, we perform waterflood simulations for oil-wet and water-wet wettability scenarios for sequential and distributed computations. Finally, we compare the relative permeability curves obtained from distributed computations to the reference relative permeability obtained from sequential simulations.

Figure 6 and Figure 7 show that the relative permeability curves obtained from distributed computations were in good agreement with the reference sequential simulation for both networks and for the considered wettability scenarios. However, we point out that the parallelization introduces a small discrepancy with the sequential runs close to Sor for the water-wet cases. This is expected as Sor is controlled by the trapping in this case and a small perturbation of the filling order induced by the parallelization would impact the Sor. For the oil-wet case, there was a good agreement in the Sor between the sequential and parallel runs, as for this wettability scenario, the Sor is mainly controlled by the collapse of oil layers which is directly linked to the Pc value. In the formulation of our parallel algorithm, we took cautious care to have the same Pc in all the parallel process and thus we could achieve a good agreement in Sor for this case. Nevertheless, we observe a small discrepancy in the Krw for low water saturations in the parallel runs compared to the reference run. This could be explained by the fact that, waterflood in an oil-wet rock is a physical drainage process, leading to an invasion percolation waterflood regime. It is well known that invasion percolation is an unstable invasion process where the injected fluid goes into the pore elements with the lowest capillary entry pressure and unlike imbibition processes where the waterfront is stabilized with cooperative pore filling, a capillary fingering flow regime is obtained. This flow regime creates a fast increase of the water relative permeability once water finger reaches the outlet. A small perturbation of the filling order caused by the temporary decoupling of the computations during the parallelization can lead to discrepancy we observe in Krw.

Although a small discrepancy was observed between the sequential and parallel runs, a very good agreement was observed in the presented cases. We highlight that the presented validation cases are not the simplest for the parallelization as the networks were relatively small (comparing to the ones used in the paper) and were divided into relatively small domains (down to 7800 elements per CPU). In this work, we will use larger subnetworks for each CPU to have more efficient parallelization and to keep higher accuracy of the results.

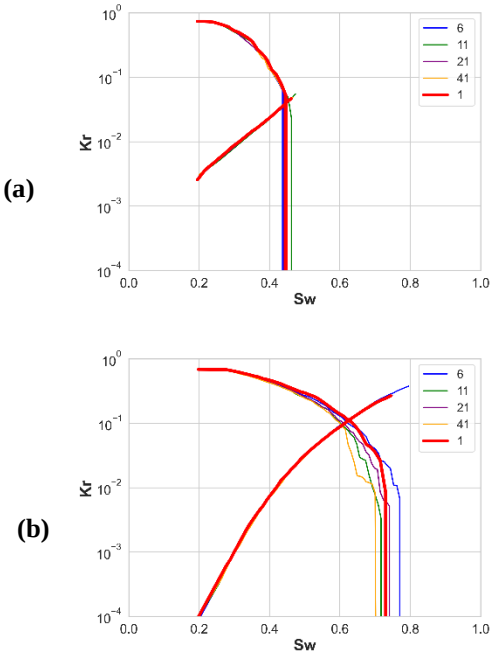

Figure 6: Comparison between waterflood kr for a WW case with a varying number of CPUs for Reservoir Carbonate C (a) and Reservoir Sandstone B (b)

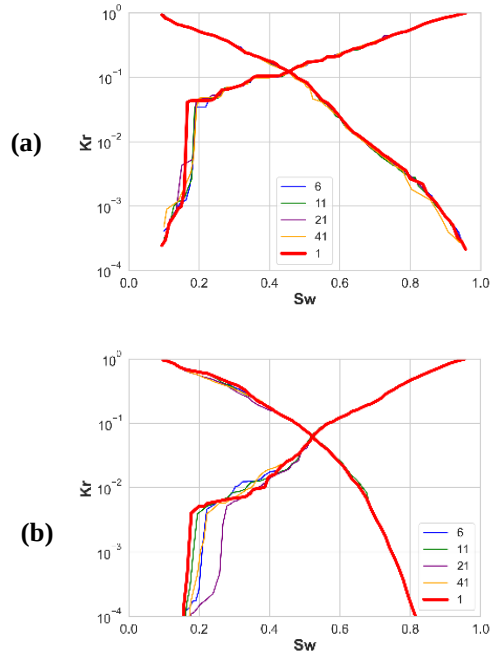

Figure 7 Comparison between several waterflood kr for a OW case with a varying number of CPUs for Reservoir Carbonate C (a) and Reservoir Sandstone B (b)

2.2.2 Change of film flow hypothesis

Wettability is a key parameter in two-phase flow in porous media. Therefore, it is critical that any pore scale simulation technique can reproduce, at least qualitatively, the trends of the effects of a wettability change on relative permeability. Craig [8] presented the key features of strongly oil-wet and strongly water-wet relative permeability curves and their typical shapes. He showed that water relative permeability is higher in the strongly oil-wet case compared to the strongly water-wet case. Moreover, he exposed that oil relative permeability in the oil-wet case is lower than that in the water-wet case. We would like to emphasize here that these are rules of thumbs for extreme wettability conditions. Several SCAL subsequent studies have agreed with these rules [18, 19, 21, 23] and the same qualitative behavior was observed between extreme wettability conditions. However, the PNM literature showed otherwise, and the behavior of the oil-wet water relative permeability curves was very different from the behavior and shape of the SCAL curves. In fact, in several modelling studies in the literature [1, 7, 36] , the relative permeability of water in oil-wet scenarios was seen to stay very low until high water saturations. This is not consistent with experimental SCAL studies of relative permeability in strongly oil-wet scenarios [18] and it can cause a counter-intuitive trend leading to having relative permeability of water in strongly oil-wet scenario lower than the one in water-wet case [7, 36] which is inconsistent with Craig's rules and the experimental studies that have confirmed them.

McDougall and Sorbie [20] studied the impact of wettability on the relative permeability and their simulations were consistent with Craig's rule. They have seen that strongly oil-wet water relative permeability curves were higher than strongly water-wet ones. They have also observed that the opposite behaviour occurs for oil relative permeability. Unlike the previously cited PNM models McDougall and Sorbie [20] did not use the sandwiched layer model [15, 22, 34], they used instead a simpler pore network bonds model statistically generated with simplified layer physics. Besides, they started their simulations with no initial water in their network.

We propose that the inconsistency is caused by a historical modelling artefact in most PNM models which led to studies that showed the counter-intuitive behavior in Krw in oil-wet systems.

Most of the models in the literature use the sandwiched oil layers model in which water layers remain in the corners in oil-wet pores after aging. This means that the water from Swi is connected to the inlet through these layers which allows invasions starting from the Swi. These invasions would increase the water saturation in the system during a waterflood without increasing the connectivity of the water between inlet and outlet thus resulting in very low water relative permeability curves until water saturations of 70% -80% (not observed experimentally). However, these layers have very small conductivity and are not able to transport large quantities of water.

This issue has been fixed in DynaPNM by disabling the connections of the water through the films in oil-wet pores and throats. This change in the layer modelling hypothesis had a large impact on water relative permeability in oil wet simulations (as we can see in the example of Figure 8). The water relative permeability increases very early in waterflood.

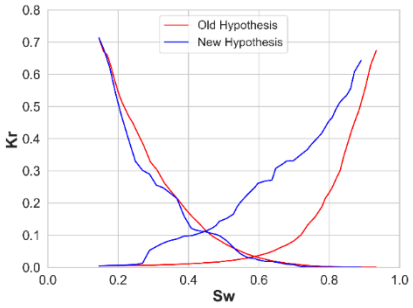

Figure 8 :Comparison between waterflood relative permeability curves for an oil-wet simulation on Reservoir Sandstone A network using the old (red) films connectivity hypothesis and the new one (blue)

2.2.3- Statistical uncertainty workflow

Sorbie and Skauge [32] have explained that several input parameters of pore network simulation are uncertain and presented the wettability assignment step as the most complex and least validated stage of the DRP workflow. There are other uncertain parameters of the DRP such as the amount of clay and the network used in the simulation (i.e. for some rocks, selected networks from different locations could give different simulation results). These uncertainties have been used by some researchers in the past in order to "tune" the simulation results to SCAL relative permeability curves. However, if one wants to be predictive, s/he should not know the result a priori and this makes choosing the uncertain parameters tricky. Therefore, we have developed a statistical uncertainty workflow in which we vary the uncertain pore network simulation parameters (wettability distribution, contact angle spatial location, clay volume, pore network …). First, thousands of DynaPNM input files are generated in an experimental design phase using WSP method [31]. Subsequently, flow simulations are run on TOTAL's supercomputer PANGEA. This is followed by a simulation ranking exercise based on the oil production after a given amount of water injected corresponding to each Kr curve and allows us to define three scenarios:

- P10: an optimistic scenario in which only 10% of the simulations produce more than this case
- P50: a median scenario in which 50% of simulations produce more than this case
- P90: a pessimistic scenario in which 90% of the simulations produce more than this case

2.2.4- Contact angles in the simulations

Contact angle is a key input for PNM simulation as it controls the capillary entry pressures in the network. Several measurement techniques to characterize contact angles exist. Contact angle measurements from Micro-CT images of multiphase flow experiment has been very attractive recently. However, as these measurements use the 3 phase contact line for the computations, they are very sensitive to the image resolution and insufficient image resolution leads to contact angle values close to 90 degrees with very large standard deviation [33]. Furthermore, automated contact angle measurements, take into consideration the pinned menisci which are different from the contact angle input needed by a PNM simulator. Therefore, we propose in this paper a different methodology to define the contact angle input. We use qualitative information about wettability to determine possible contact angle distributions to be used. This information feeds our uncertainty analysis approach described previously and therefore the simulation produces an envelope of relative permeability curves. Unfortunately, this can lead to large envelopes of relative permeability especially in Mixed-Wet scenarios where the contact angle distribution and the spatial assignment of contact angles can have an important impact on the results. In order to decrease this uncertainty and to constrain our wettability input further, we propose to perform a fast microplug scale DRP experiment in which we reach the residual oil saturation state. The Micro-CT image at Sor is then used to constrain the simulation wettability input by removing all the realizations/ wettability inputs that are not in agreement with the Sor measured from the image. As it is well documented that Sor is correlated to wettability input [37], we think that this experiment helps us to obtain less uncertain simulation results. In the future, we plan to use additional information from the fast microplug scale experiment in order to constrain even further our PNM model.

Recent observations [11] have shown that wettability is correlated in space, and the pores having similar wettabilities are likely to be close. Furthermore, the same study has provided indications that contact angle is rather distributed following two distributions in aged samples. Therefore, we consider a fractional wettability model having two contact angle distributions with spatial correlation in our mixed-wet simulations.

3- Results

3.1. Wettability impact on relative permeability

Having built the DRP workflow, we proceed to its validation. As a first test, we would like to test if the PNM simulations agree with the widely used Craig's rules of thumbs [8]. As mentioned earlier in the paper, unlike the SCAL literature, the PNM literature provides different trends and we think that it is the result of a historical modelling artefact. We run strongly water-wet and strongly oil-wet simulations on several networks. We report in Figure 9 and Figure 10 two examples of our results for Reservoir Sandstone A and Reservoir Sandstone B. We notice that our simulations reproduce well the Craig's rule of thumb. Water relative permeability was higher in the strongly oil-wet simulation compared to the strongly water-wet one. Moreover, oil relative permeability was lower in the oil-wet case compared to the water-wet simulation.

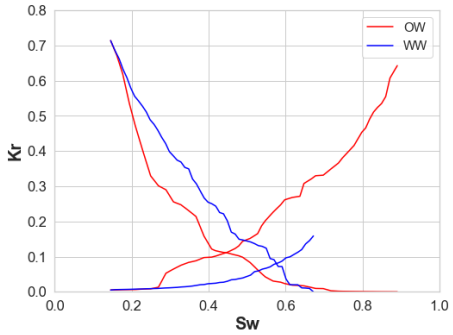

Figure 9 : Comparison between waterflood kr of strongly water-set with constant contact angle equal to 50° (blue) and strongly oil-wet with constant contact angle equal to 150° (red) simulations on Reservoir Sandstone A pore network

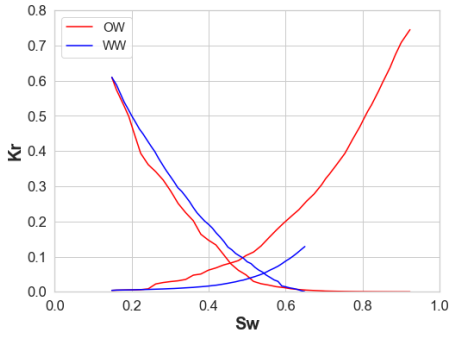

Figure 10 : Comparison between waterflood kr of strongly WW with constant contact angle equal to 50° (blue) and strongly OW with constant contact angle equal to 150° (red) simulations on Reservoir Sandstone B pore network

3.2. Validation of DRP workflow against microplug experiments

In the last years, new techniques to perform steady-state relative permeability experiments at microplug scale have been developed [5, 12, 13, 16] allowing Kr measurements simultaneously with imaging of the fluids. These datasets are very suitable to validate pore scale simulators as they enable the simulation of the same volume used in the experiment. Furthermore, this data is rich and helps understand the limitations of the DRP simulation in case of discrepancy. We simulate three microplug simulations in this section in order to validate the physics in our simulator. In the three datasets, only a 1 cm long section was scanned at a resolution a priori acceptable for PNM simulations. Therefore, we propose to perform the simulations on this section and compare the simulation results to relative permeability curves estimated using DNS from the experiment multiphase images (called 'experimental' Kr in this section). Although the computed relative permeabilities would be limited by the image resolution, they allow us to compare simulated and 'experimental' Kr curves from the exact same volume and prevent discrepancies caused by the heterogeneity of the samples and/or by differences in the aspect ratios between the experiment and the simulated system.

To estimate the 'experimental' relative permeability curves from the multiphase flow images, we first segment the images to identify the voxels filled with oil, water and grain. This step has some uncertainty as a segmentation is biased by user decisions. Then, a pressure gradient is applied between the inlet and outlet for each phase separately, and single phase OpenFOAM simulations are performed. The computed flow rate obtained for each phase is then used to compute the effective permeability of each phase using Darcy's law and finally relative permeability curves are obtained by dividing the effective permeabilities by the absolute permeability. When the raw images of the experiments are available, we perform an uncertainty analysis on the segmentation to have an idea about the 'experimental' uncertainty.

Wettability is a key input for a PNM simulation and as discussed previously we use qualitative wettability information from the experiment as a first input to our experimental design usually resulting in large envelope of relative permeability curves especially for mixed-wet scenarios. Then, we constrain this input by only selecting the realisations that agree with the Sor of the steady-state experiments.

The first dataset that we consider is Reservoir Sandstone rock A without aging. The microplug experiment showed water-wet (WW) behavior characteristics [13]. Therefore, we have used the wettability input in Table 1. In our experimental design, 10000 realizations have been generated and simulated (with varying the seeds numbers, the parameters of the contact angle distributions as described in table 1 and wettability spatial correlation parameters). Next, only the realizations in agreement with Sor (difference less than 5%) have been kept. Finally, the results have been ranked at 10 PV injected and, P10, P50 and P90 scenarios were established. Figure 11 shows that the simulated relative permeabilities agree well with the experimental curves. We point out that the experimental Swi depends on the segmentation of the experimental images. As we performed an experimental uncertainty analysis that takes into account the various segmentations, we could find a range of Swi values. For simplicity, we only considered Swi in the simulation (as an input parameter) from the base case experimental images segmentation.

Table 1 : Waterflood wettability parameters used in simulations of WW Reservoir Sandstone A

	Value/Range
WF advancing contact angle distribution	Normal distribution
WF advancing contact angle standard deviation	1°-10°
Mean advancing WF contact angle	50°-80°

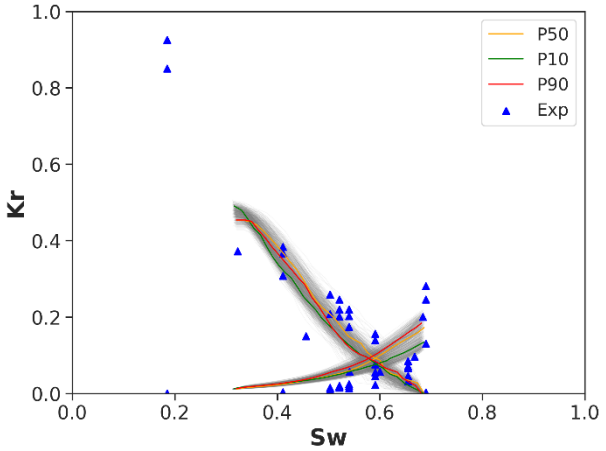

Figure 11: Comparison between simulated and 'experimental' (computed from experimental images at several fw) relative permeability curves for WW Reservoir Sandstone A

Then, we simulate a second dataset of Reservoir Sandstone A with aging. The microplug experiment showed mixed-wet (MW) behavior characteristics [13]. We have then used the simulation workflow described above and the wettability input of Table 2. Figure 12 shows that the simulated oil relative permeability is within the experimental envelope. The water relative permeability is in good agreement with the experimental curve for low and medium saturation values but is slightly higher close to Sor.

Table 2 : Waterflood wettability parameters used in simulations of MW Reservoir Sandstone A

	Value/Range
WF advancing contact angle distribution	Normal distribution
WF dist1, advancing contact angle standard deviation	1°-10°
Mean advancing WF dist1 contact angle	100°-130°
WF dist 2 advancing contact angle distribution	normal
WF dist2, advancing contact angle standard deviation	5°- 20°
Mean advancing WF dist2 contact angle	91°-100°
Fraction of distribution 2	0.35-0.75
Correlation length	3-5

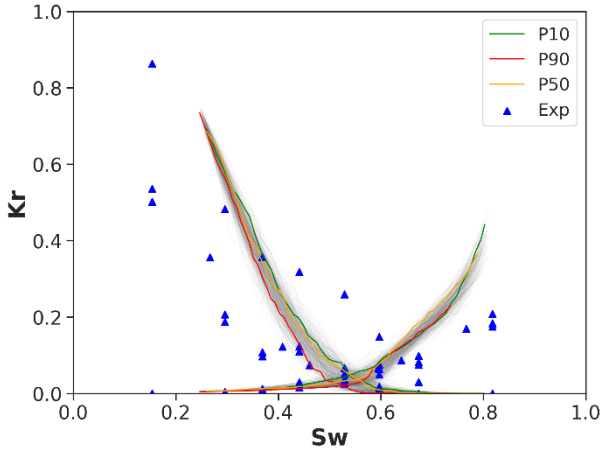

Figure 12: Comparison between simulated and 'experimental'(computed from experimental images at several fw) relative permeability curves for MW Reservoir Sandstone A

Finally, we simulate a dataset of Bentheimer with aging. The microplug experiment showed mixed-wet behavior characteristics [17]. We have then used the simulation workflow described above and the wettability input of

Table 3. Figure 13 shows that the simulated water relative permeability is in good agreement with the experiment. The simulated oil relative permeability is however slightly higher than the experimental values. Unfortunately, we didn't have access to the grey scale images of this experiment and therefore could not establish the experimental uncertainty for this dataset.

Overall, the agreement was satisfactory between the three datasets and our simulation results.

Table 3 : Waterflood wettability parameters used in simulations of MW Bentheimer

	Value/Range
WF advancing contact angle distribution	Normal distribution
WF dist1, advancing contact angle standard deviation	5°-20°
Mean advancing WF dist1 contact angle	110°-140°
WF dist 2 advancing contact angle distribution	normal
WF dist2, advancing contact angle standard deviation	5°- 10°
Mean advancing WF dist2 contact angle	75°-100°
Fraction of distribution 2	0.5-0.65
Correlation length	4-6

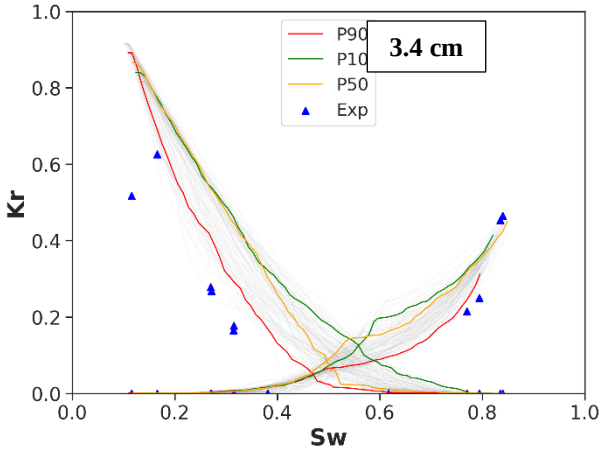

Figure 13: Comparison between simulated and 'experimental' (computed from experimental images at several fw) relative permeability curves for MW Bentheimer

3.3. Large scale simulations

We present in this section an example of large-scale simulations on Bentheimer. We start from an image of Bentheimer (560*560*10000) acquired at 4 microns resolution. We extract a pore network from this image from 13 extractions stitched together. This results in a pore network with 242k elements (Figure 14). Although this network is not small, our PNM simulator can handle much larger volumes. Therefore, we perform several PNM duplications by periodicity in the lateral direction in order to achieve large volumes. The original and duplicated networks are linked together via newly generated throats with Delaunay triangulation algorithm [9]. After 16 duplications in each lateral direction, we obtain a pore network having 63 million elements, representing an image of 8480*8480*10000 voxels and representing a physical volume of 46 cm^3 which is a typical size of plugs used in MICP measurements.

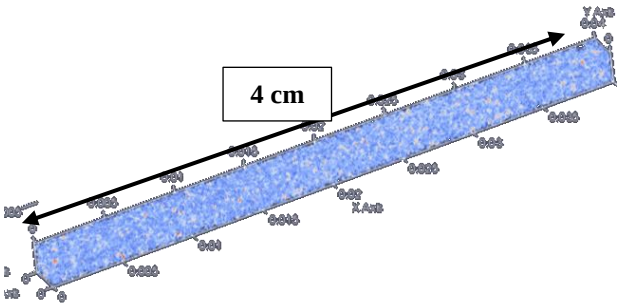

*Figure 14 : Bentheimer pore network obtained by 13 stitched extractions from 560*560*10000 voxels image*

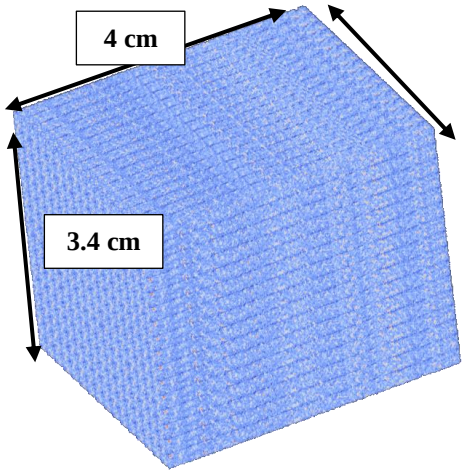

*Figure 15 : Bentheimer pore network obtained from lateral multiplication of network of Figure 14. This network represents an image of 8480*8480*10000 voxels*

The parallelization of our flow simulator resulted in faster computations and made large networks simulations possible. For instance, simulating a primary drainage, followed by waterflood with Kr computations on the large Bentheimer network (Figure 15) took 6.5 hours with 81 CPUs. This simulation was two orders of magnitude faster than a sequential simulation on the same network. Figure 16 shows the simulation time evolution by varying number of CPUs used. We see that the simulation time decreases very fast with more CPUs to reach an optimal speed-up for 81 cores. Then, it stabilizes and starts increasing meaning that the number of pore elements in each core domain becomes too small to take advantage of the parallelization.

These are, to our knowledge, the largest PNM simulations (in terms of number of pore elements) ever reported in the literature. We think that we can even simulate larger networks as we did not reach yet the limits of our PNM simulator.

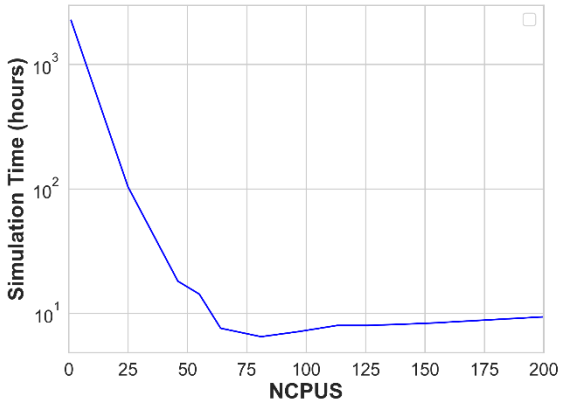

Figure 16 : Simulation time on 21 million pore bodies network (representing 46cm3 volume) as a function of the number of CPUS

Being able to simulate large volumes enables us to investigate the impact of image size used in DRP on the dispersion of the results. We crop several networks from a large Bentheimer network obtained as described above.

Subsequently, we simulate primary drainage and waterflood on several realizations of each cropped pore network. Figure 17, Figure 18 and Figure 19 show that the larger the image/network the smaller the variability. This reduction of the dispersion is both due to the reduction of the finite size effect as the number of elements in the network increases and by the fact that more heterogeneity is taken into account in the larger pore networks being closer to REV. However, it is difficult to speak about REV for this case as we are limited by the information available from the image.

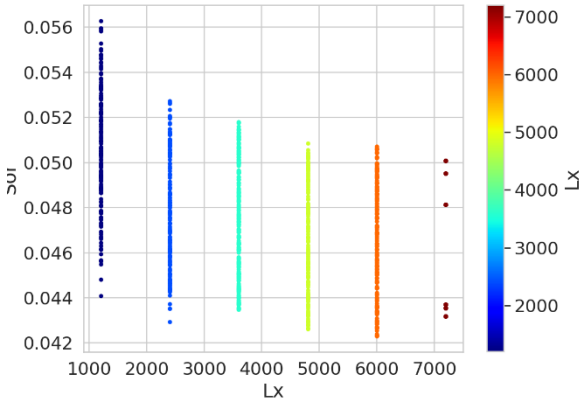

Figure 17: Evolution of the Sor dispersion with varying size of Bentheimer cubic image for an oil-wet system

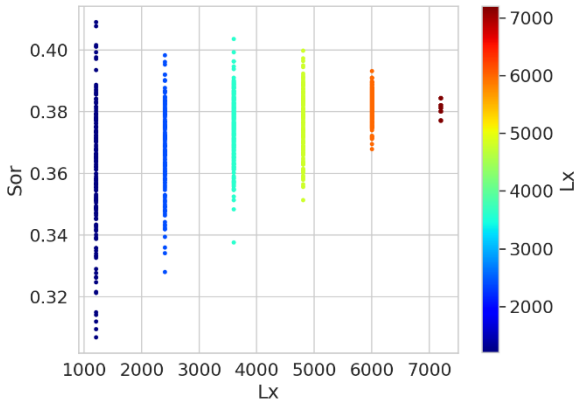

Figure 18: Evolution of the Sor dispersion with varying size of Bentheimer cubic image for a water-wet system

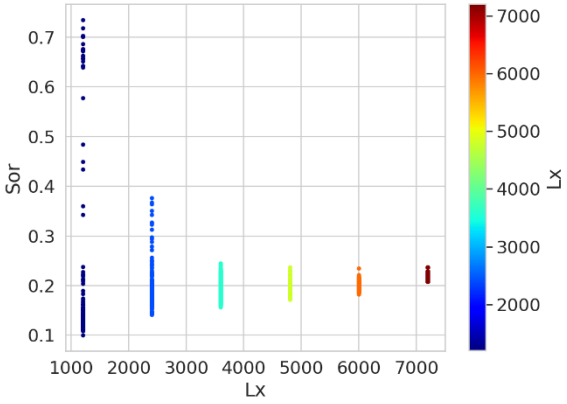

Figure 19 : Evolution of the Sor dispersion with varying size of Bentheimer cubicimage for a mixed-wet system

3.4. Validation of DRP workflow against SCAL experiment

Having validated our PNM simulations against microplug experiments, we perform a comparison against a SCAL experiment performed on Reservoir Sandstone B. We acquired an image of size 1300*1300*6358 voxels at 1.5 microns resolution and extracted a pore network having 1.7 million pore elements. To avoid adding bias to our simulations, we propose to use the same aspect ratio as the experiment (equal to 5), and we avoid making network duplications along the flow direction. As our image has the same aspect ratio as the experiment, the largest network that we could use is the network extracted from the full image. First, we check if we reach reasonable dispersion using this network. The full sample image is equivalent to a 2200^3 image and we observe that for OW and WW the Sor value had stabilized and that the dispersion became reasonable.

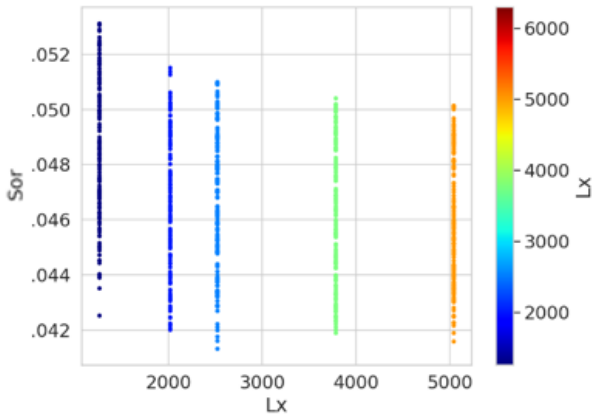

Figure 20 : Evolution of the Sor dispersion with varying size of Reservoir Sandstone B cubic image for an oil-wet system

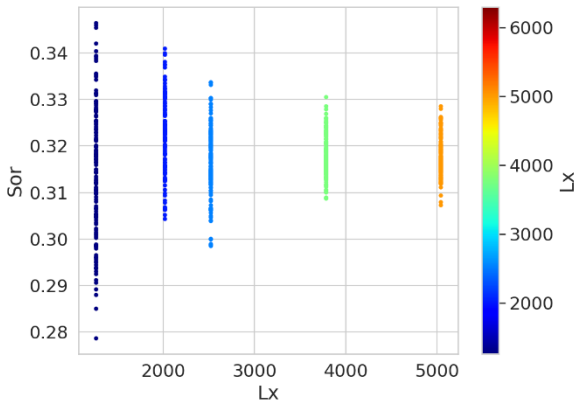

Figure 21 : Evolution of the Sor dispersion with varying size of Reservoir Sandstone B cubic image for a water-wet system

The SCAL experiment has shown water-wet or mixed-wet with large water-wet characteristics. In fact, the oil production was fast and the Sor was high. Therefore, this qualitative information has been used in the simulation. An experimental design was used to generate 1996 realizations. These were run using DynaPNM, the simulated relative permeability curves were ranked at 10 PV injected and, P10, P50 and P90 scenarios were subsequently established. We did not have a microplug experiment for this dataset, therefore we did not use the Sor image to discard some realizations and we report here all the simulated 1996 realizations. Figure 22 shows that the simulated relative permeabilities is in good agreement with the experimental Kr curve. Furthermore, Figure 23 shows that the simulated Sor was close to the experimental residual oil saturation. This gives us confidence of the robustness of our simulation workflow. Although, the agreement was good between the simulations and experiment for this sample without using Sor image of a fast experiment to constrain the wettability input in the simulation, we do not think that this result is guaranteed and we believe that for different cases – especially for mixed-wet cases with more oil-wet fraction, that an experimental input is needed to keep the uncertainty of the PNM simulations reasonable.

Table 4 : Wettability parameters used in the simulation of the SCAL experiment performed on Reservoir Sandstone B

	Value/Range
WF advancing contact angle distribution	Normal distribution
WF dist1, advancing contact angle standard deviation	4°-8°
Mean advancing WF dist1 contact angle	100°-120°
WF dist 2 advancing contact angle distribution	normal
WF dist2, advancing contact angle standard deviation	4°- 8°
Mean advancing WF dist2 contact angle	40°-75°
Fraction of distribution 2	0.65-0.99
Correlation length	1-6

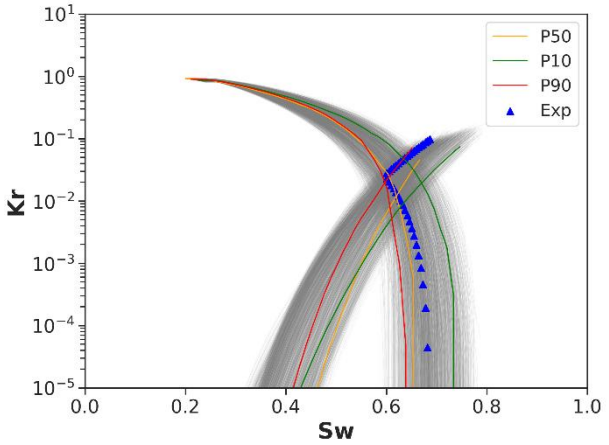

Figure 22 : Comparison between simulated and SCAL experimental relative permeability curves for Reservoir Sandstone B

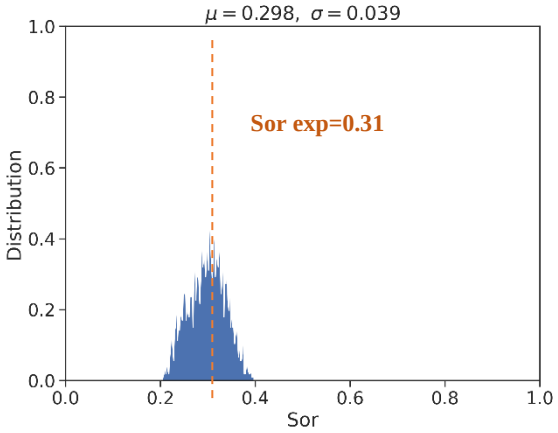

Figure 23: Comparison between simulated (blue) and experimental (orange) Sor value for Reservoir Sandstone B

4- Conclusions

In this paper, we have presented TOTAL's DRP workflow for multiphase flow simulation and relative permeability estimation. First, an upscaled version of the segmented image was built in the form of a pore network with single phase Direct Numerical Simulation performed to compute the conductivities of the pores. This allows us to get the accuracy of DNS and the computational efficiency of PNM. The network extraction was then completed by a stitching algorithm that allows the extraction of larger volumes and overcome the memory limitations of the extraction code. This network feeds our in-house pore network simulator DynaPNM. The parallelization of DynaPNM unlocked the simulations on networks with tens of million pore elements in few hours and made possible the simulation of plug scale volumes (with few microns resolution). These simulations are to our knowledge the largest PNM simulations (in terms of number of pore elements) ever reported in the literature.

We have made a change in the way to model water films in oil-wet pores to correct a historical modeling artefact in

PNM which is seen to have a very large impact on simulation accuracy in oil-wet and mixed-wet scenarios.

After this change, we show that our simulation workflow reproduced the relative permeability trends with respect to changes of wettability that are consistent with the well-known Craig's rule. Subsequently, we have validated our simulations against three relative permeability experiments performed on microplugs and against a SCAL dataset. The agreement was satisfactory for all cases; however, more validation work is required to test further the robustness of the workflow for more rocks and wettability configurations.

For the future, we plan to constrain further our PNM simulations in order to reduce the uncertainty and dispersion in our results. We would also like to have more heterogeneity information in our simulations by using larger rock images.

Acknowledgements

The authors would like to thank TOTAL management for the authorization to publish this work. Dr. Franck Nono, Régis Brugidou and Dr. Maria Repina are acknowledged for acquiring and processing some of the images used in this work. We would like to thank Dr Branko Bijeljic, Dr Ali Raeini and Prof. Martin Blunt for the technical discussions and providing some experimental data used in this study.

References

1. Al-Futaisi, A., Patzek, T.W.: Secondary imbibition in NAPL-invaded mixed-wet sediments. Journal of contaminant hydrology **74**(1-4), 61–81 (2004)
2. Alhammadi, A.M., AlRatrout, A., Singh, K., Bijeljic, B., Blunt, M.J.: In situ characterization of mixed-wettability in a reservoir rock at subsurface conditions. Scientific Reports **7**(1), 1–9 (2017)
3. AlRatrout, A., Raeini, A.Q., Bijeljic, B., Blunt, M.J.: Automatic measurement of contact angle in pore-space images. Advances in Water Resources **109**, 158–169 (2017). doi: 10.1016/j.advwatres.2017.07.018
4. Andrew, M., Bijeljic, B., Blunt, M.J.: Pore-scale contact angle measurements at reservoir conditions using X-ray microtomography. Advances in Water Resources **68**, 24–31 (2014)
5. Bagudu, U., McDougall, S.R., Mackay, E.J.: Pore-to-Core-Scale Network Modelling of CO2 migration in Porous Media. Transport in Porous Media **110**(1), 41–79 (2015). doi: 10.1007/s11242-015-0556-z
6. Balay, S., Abhyankar, S., Adams, M., Brown, J., Brune, P., Buschelman, K., Dalcin, L., Dener, A., Eijkhout, V., Gropp, W.: PETSc users manual (2019)
7. Bondino, I., Hamon, G., Kallel, W., Kac, D.: Relative Permeabilities From Simulation in 3D Rock Models and Equivalent Pore Networks: Critical Review and Way Forward1. SPWLA-2012-v53n6a2 **54**(06), 538–546 (2013)
8. Craig, F.F.: The reservoir engineering aspects of waterflooding, vol. 3. HL Doherty Memorial Fund of AIME New York (1971)
9. Delaunay, B.: Sur la sphere vide. Izv. Akad. Nauk SSSR, Otdelenie Matematicheskii i Estestvennyka Nauk **7**(793-800), 1–2 (1934)
10. Dong, H., Blunt, M.J.: Pore-network extraction from micro-computerized-tomography images. Physical review E **80**(3), 36307 (2009)
11. Foroughi, S., Bijeljic, B., Lin, Q., Raeini, A.Q., Blunt, M.J.: Pore-by-pore modeling, analysis, and prediction of two-phase flow in mixed-wet rocks. Phys. Rev. E **102**(2), 23302 (2020). doi: 10.1103/PhysRevE.102.023302
12. Gao, Y., Lin, Q., Bijeljic, B., Blunt, M.J.: X-ray Microtomography of Intermittency in Multiphase Flow at Steady State Using a Differential Imaging Method. Water Resour. Res. **53**(12), 10274–10292 (2017). doi: 10.1002/2017WR021736
13. Gao, Y., Raeini, A.Q., Selem, A.M., Bondino, I., Blunt, M.J., Bijeljic, B.: Pore-scale imaging with measurement of relative permeability and capillary pressure on the same reservoir sandstone sample under water-wet and mixed-wet conditions. Advances in Water Resources **146**, 103786 (2020). doi: 10.1016/j.advwatres.2020.103786
14. Gropp, W., Gropp, W.D., Lusk, E., Lusk, Argonne Distinguished Fellow Emeritus Ewing, Skjellum, A.: Using MPI: portable parallel programming with the message-passing interface, vol. 1. MIT press (1999)
15. Kovscek, A.R., Wong, H., Radke, C.J.: A pore-level scenario for the development of mixed wettability in oil reservoirs. AIChE Journal **39**(6), 1072–1085 (1993)
16. Lin, Q., Bijeljic, B., Pini, R., Blunt, M.J., Krevor, S.: Imaging and Measurement of Pore-Scale Interfacial Curvature to Determine Capillary Pressure Simultaneously With Relative Permeability. Water Resour. Res. **54**(9), 7046–7060 (2018). doi: 10.1029/2018WR023214
17. Lin, Q., Bijeljic, B., Berg, S., Pini, R., Blunt, M.J., Krevor, S.: Minimal surfaces in porous media: Pore-scale imaging of multiphase flow in an altered-wettability Bentheimer sandstone. Physical review E **99**(6), 63105 (2019)
18. Masalmeh, S.K. (ed.): The Effect of Wettability on Saturation Functions and Impact on Carbonate Reservoirs in the Middle East. Society of Petroleum Engineers (2002)
19. Mascle, M., Youssef, S., Deschamps, H., Vizika, O.: In-Situ Investigation of Aging Protocol Effect on Relative Permeability Measurements Using High-Throughput Experimentation Methods. SPWLA-2012-v53n6a2 **60**(04), 514–524 (2019)
20. McDougall, S.R., Sorbie, K.S.: The Impact of Wettability on Waterflooding: Pore-Scale Simulation. SPE-25271-PA **10**(03), 208–213 (1995). doi: 10.2118/25271-PA
21. Morrow, N.R., Cram, P.J., McCaffery, F.G.: Displacement studies in dolomite with wettability control by octanoic acid. Society of Petroleum Engineers Journal **13**(04), 221–232 (1973)
22. Oren, P.-E., Bakke, S., Arntzen, O.J.: Extending predictive capabilities to network models. SPE journal **3**(04), 324–336 (1998)

23. Owens, W.W., Archer, D.: The effect of rock wettability on oil-water relative permeability relationships. Journal of Petroleum Technology **23**(07), 873–878 (1971)
24. Raeini, A.Q., Blunt, M.J., Bijeljic, B.: Modelling two-phase flow in porous media at the pore scale using the volume-of-fluid method. Journal of Computational Physics **231**(17), 5653–5668 (2012). doi: 10.1016/j.jcp.2012.04.011
25. Raeini, A.Q., Bijeljic, B., Blunt, M.J.: Generalized network modeling of capillary-dominated two-phase flow. Physical review. E **97**(2-1), 23308 (2018). doi: 10.1103/PhysRevE.97.023308
26. Raeini, A.Q., Yang, J., Bondino, I., Bultreys, T., Blunt, M.J., Bijeljic, B.: Validating the Generalized Pore Network Model Using Micro-CT Images of Two-Phase Flow. Transport in Porous Media **130**(2), 405–424 (2019). doi: 10.1007/s11242-019-01317-8
27. Regaieg, M., Moncorgé, A.: Adaptive dynamic/quasi-static pore network model for efficient multiphase flow simulation. Computational Geosciences **21**(4), 795–806 (2017)
28. Ryazanov, A.V., van Dijke, M.I.J., Sorbie, K.S. (eds.): Pore-network prediction of residual oil saturation based on oil layer drainage in mixed-wet systems. Society of Petroleum Engineers (2010)
29. Saxena, N., Hofmann, R., Alpak, F.O., Dietderich, J., Hunter, S., Day-Stirrat, R.J.: Effect of image segmentation & voxel size on micro-CT computed effective transport & elastic properties. Marine and Petroleum Geology **86**, 972–990 (2017)
30. Scanziani, A., Singh, K., Blunt, M.J., Guadagnini, A.: Automatic method for estimation of in situ effective contact angle from X-ray micro tomography images of two-phase flow in porous media. Journal of colloid and interface science **496**, 51–59 (2017). doi: 10.1016/j.jcis.2017.02.005
31. Sergent, M.: Contribution de la Méthodologie de la Recherche Expérimentale à l'élaboration de matrices uniformes: Application aux effets de solvants et de substituants. Aix-Marseille 3 (1989)
32. Sorbie, K.S., Skauge, A.: Can Network Modeling Predict Two-Phase Flow Functions? SPWLA-2012-v53n6a2 **53**(06), 401–409 (2012)
33. Sun, C., McClure, J.E., Mostaghimi, P., Herring, A.L., Meisenheimer, D.E., Wildenschild, D., Berg, S., Armstrong, R.T.: Characterization of wetting using topological principles. Journal of colloid and interface science **578**, 106–115 (2020)
34. Valvatne, P.H., Blunt, M.J.: Predictive pore-scale modeling of two-phase flow in mixed wet media. Water Resour. Res. **40**(7) (2004)
35. Yang, J.: Multi-scale simulation of multiphase multi-component flow in porous media using the Lattice Boltzmann Method (2013)
36. Zhao, X., Blunt, M.J., Yao, J.: Pore-scale modeling: Effects of wettability on waterflood oil recovery. JOURNAL OF PETROLEUM SCIENCE AND ENGINEERING **71**, 169–178 (2010). doi: 10.1016/j.petrol.2010.01.011
37. Zhou, X., Morrow, N.R., Ma, S.: Interrelationship of wettability, initial water saturation, aging time, and oil recovery by spontaneous imbibition and waterflooding. SPE journal **5**(02), 199–207 (2000)